Environ Earth Sci (2015) 73:8125–8143
DOI 10.1007/s12665-014-3971-5

ORIGINAL ARTICLE

Electrical resistivity imaging for aquifer mapping over Chikotra basin, Kolhapur district, Maharashtra

Gautam Gupta · J. D. Patil · Saumen Maiti · Vinit C. Erram · N. J. Pawar · S. H. Mahajan · R. A. Suryawanshi

Received: 19 December 2013 / Accepted: 18 December 2014 / Published online: 1 January 2015

Abstract Electrical resistivity study assumes a special significance for mapping aquifers in hard rock areas. A two-dimensional (2D) resistivity survey of Chikotra basin, southern part of Kolhapur district in the Deccan Volcanic Province of Maharashtra was conducted. The aim of this work was to determine the aquifer zones of the study area using electrical resistivity imaging technique. The hydrogeological section derived from the available dug well/borehole lithology suggests that the top layer comprises red bole, laterite or black soil followed by weathered/fractured rock grading into compact basalts. The sources of groundwater appear to be available in weathered and fractured basalt trapped between weathered overburden and hard rock. Results from the 2D inverted models of resistivity variation with depth suggest the occurrence of aquifers mostly in weathered/fractured zones within the traps or beneath it. The resistivity models suggest that the northern part of the study area represents a promising aquifer zone with reasonable thickness of weathered basement. The models further indicate that there are several locations throughout the basin for possible groundwater exploration as it exhibited strong water-bearing potential in the subsurface rocks.

Keywords Aquifers · Electrical resistivity imaging (ERI) · Groundwater · Chikotra basin · Deccan Volcanic Province · Maharashtra

G. Gupta (✉) · V. C. Erram · S. H. Mahajan
Indian Institute of Geomagnetism, New Panvel (W), Navi Mumbai 410218, India
e-mail: gupta_gautam1966@yahoo.co.in

J. D. Patil
D.Y. Patil College of Engineering and Technology, Kasaba Bawada, Kolhapur 416006, India

S. Maiti
Department of Applied Geophysics, Indian School of Mines, Dhanbad 826004, India

N. J. Pawar
Shivaji University, Vidyanagar, Kolhapur 416004, India

R. A. Suryawanshi
Yashwantrao Chavan College of Science, Karad-Masur Road, Karad 415124, India

Introduction

Groundwater is the main resource of water supply required for industrial, agricultural and domestic purposes in many semi-arid regions. In some cases, over-exploitation has caused declining groundwater levels and has consequently limited groundwater flow to deeper weathered/fractured zones (Rai et al. 2011; Kumar et al. 2011; Maiti et al. 2012). In view of the depleting conditions of water resources in Maharashtra and increasing demands of water for meeting the requirements of the rapidly growing population, as well as the problems that are expected to arise in the future, a holistic, well-planned long-term strategy is needed for sustainable groundwater resource assessment and management.

Of all non-intrusive surface geophysical techniques, the electrical resistivity imaging (ERI) method has been applied most widely to obtain subsurface information due to the wide range of resistivity for different geological materials (Keller and Frischknecht 1966; Bhattacharya and Patra 1968; Koefoed 1979). Particularly, the resistivity method has been effectively used by a number of researchers in various fields of application including groundwater investigations (Devi et al. 2001; Lenkey et al.

2005; Hamzah et al. 2007; Gupta et al. 2012; Maiti et al. 2012, 2013a), groundwater contamination studies (Karlik and Kaya 2001; Frohlich et al. 2008; Kundu and Mandal 2009; Park et al. 2007; Mondal et al. 2013), saltwater intrusion problems (Edet and Okereke 2001; Hodlur et al. 2006; Song et al. 2007; Hermans et al. 2012; Maiti et al. 2013b), geothermal explorations (El-Qady et al. 2000; Kumar et al. 2011). This technique helps to delineate top soil, weathered, fractured and bedrock zone for construction of suitable groundwater units, because in hard rock terrain, the weathered and fractured zone constitutes the potential loci for groundwater flow (Maiti et al. 2012). Thus, delineation of aquifers is the pre-requisite for the assessment of regional/local groundwater potential. Several researchers have carried out systematic hydro-geological and geophysical investigations in the Deccan Trap region (Bose and Ramkrishna 1978; Deolankar 1980; Singhal 1997; Pawar et al. 2009; Rai et al. 2011, 2013; Ratnakumari et al. 2012) to delineate fracture zones within the trap sequence and sedimentary formations below the traps, which are considered to be a potential resource of groundwater.

The present study attempts to define the aquifer zones within the weathered/fractured basaltic rocks as well as below the traps in the Chikotra basin of the Deccan Volcanic Province (DVP) of Kolhapur district for groundwater investigation using multi-electrode resistivity imaging technique. Generally in the Trap country, fluviatile and lacustrine deposits are formed during the interval between successive lava flows. These sedimentary deposits are known as intertrappean beds. Each lava flow is composed of vesicular basalt unit on top and compact basalt unit at the bottom. Intertrappean beds together with the underlying vesicular basalt units form groundwater prospective zones between two compact basalt layers (Rai et al. 2013). Ghosh et al. (2006) reported that if these intertrappean beds are clay rich, then it is not a prospective zone of groundwater and such beds are known as bole beds.

There are several advantages of using multi-electrode ERI system over the conventional vertical electrical technique (Dahlin 1996). This is because the multi-electrode scheme is a fast computer-aided data acquisition system and simultaneously studies both lateral and vertical changes of resistivity below the entire profile length. The ERI technique is being widely used in groundwater exploration, civil engineering, environmental and mining applications. There are, therefore, an increasing number of users for ERI technique in India and abroad for mapping accurate location of subsurface geological formations and structures like faults, fractures, joints for delineation of water-bearing zones, geothermal, etc. (Griffiths and Barker 1993; Loke and Barker 1996; Singh et al. 2006; Francese et al. 2009; Kumar et al. 2010; Zarroca et al. 2012).

The present study brings out the close relationship among the geologic, geomorphic and geoelectrical parameters of sub-surface condition for groundwater in Chikotra basin, Kolhapur district of Maharashtra. The results obtained from the present study would produce detailed groundwater condition within the basin so that the prospective locations of tube wells could be suggested in future for water resource use.

Geology and hydrogeology of the area

The study area lies in the southern part of Kolhapur district, Maharashtra (Fig. 1) and mainly covers a part of Bhudargad, Kagal and Ajara tahsils. The region selected for the present study is located between 16°10′43″ to 16°27′20″ north latitudes and 74°8′9″ to 74°22′30″ east longitudes occupying an area of about 351 km^2. The study area comprises hills on the southwestern side and plain area on the northeastern side forming irregular and diverse nature of topography.

Geologically, the basalts of the Deccan Volcanic Province characterize the Chikotra basin. In general, the basaltic flows are of simple type with maximum thickness of 35–40 m (Mungale 2001). The flows have been separated by thin clayey horizons of tuffaceous aspect called as the red boles. The thickness of the red bole varies from less than a meter to 2.5 m. In some parts (source) the topographic highs are covered with laterite and in the downstream part by a thin veneer of alluvium, which is developed along the banks of the river and streams. The thickness of the alluvium varies from 2 to 6 m. The thickness gradually increases in the downstream areas where the Chikotra River (length of the river is about 47 km) meets the Vedganga River. Its lateral extent is highly variable with maximum extent of about 500 m on either bank in the downstream part. The alluvium mainly consists of pebble beds, sand and silt derived from the Deccan Trap basalts and the laterites.

The laterite occurs in the upstream part in the source of the Chikotra River at an elevation of about 840 m above mean sea level. They occur as capping over the flat-topped basaltic hills. The basaltic bedrock show typical spheroidal weathering that gives rise to large rounded boulders on the outcrops. The weathering starts along the well-developed joints, first rounding off the angles and the corners and then producing thin concentric shells or layers, which become soft and fall off gradually. Basalts display two sets of prominent vertical as well as horizontal joints and the flows are highly jointed and fractured all over the basin. Prominent columnar joints have been observed at Murukte village. Elsewhere, like at Hasur Khurd and Khadak Ohol stream on way to Belewadi-Kalamma, the joints and

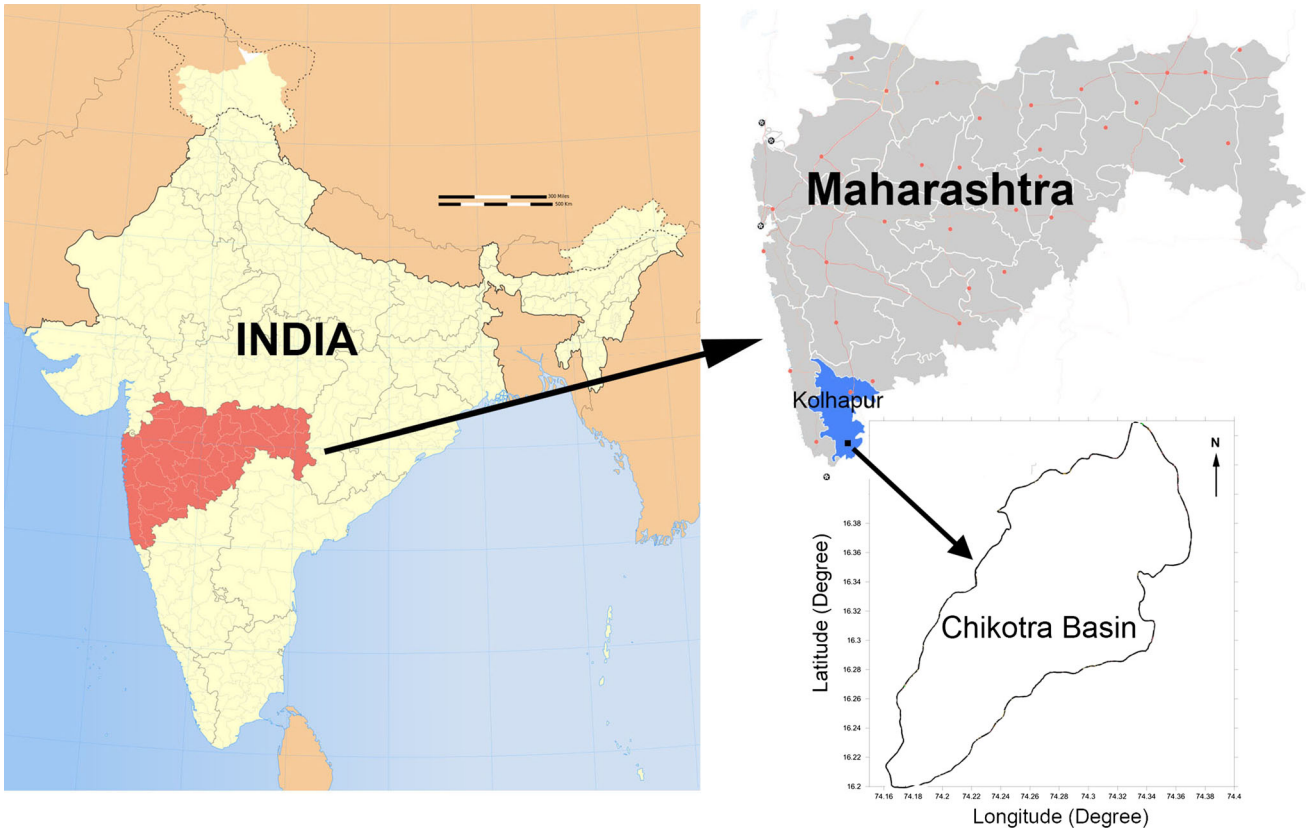

Fig. 1 Location map of Chikotra basin in Kolhapur district

fractures are profusely present. These joints attribute secondary porosity to the basalts making them potential aquifers (Deolankar 1980).

The drainage pattern is not uniform in the basin. In the upstream areas, the pattern is dendritic and fine textured. This type of drainage pattern is usually observed on horizontally disposed basaltic rock that is uniformly resistant with gentle regional slope (Horton 1945). In addition this, the laterites covering the flat-topped basaltic plateaus with slopes less than 5 % have favored the initiation of this drainage pattern. In the middle reach of the basin, the drainage represents dendritic pattern but is medium textured. This indicates that basaltic rock is characterized by joints and fractures. It can thus be inferred that rocks in the watershed are low to moderately permeable and their permeability is developing low-yielding aquifers. In the middle to lower reaches of the basin, the drainage pattern becomes sub-parallel and coarse in texture. The parallelism of the streams along a particular direction is indicative of some amount of structural control over the drainage.

In general, the area under study exhibits hilly topography. As the topography is rugged, large number of first order and second order streams are present. At some places, perennial springs are also observed at the contacts between different lithologies. They are responsible for contribution of water to the streams. In general, due to availability of water in the downstream part of Chikotra, the fertile alluvial plain is under irrigated agriculture. The basin receives an annual rainfall ranging from 1,000 to of 2,800 mm, mainly from south-west monsoon. The temperature ranges from maximum of about 40 °C in the month of May, while it is minimum of 10–15 °C in the month of November in a year.

The discharge values from the wells in the study region vary from 135 to 5,890 l/s (Mungale 2001). These values do not include the bore well discharge. These variations can be attributed to the hydraulic and morphologic characteristics of the tributaries of Chikotra River. The static water level depth in the dug wells of the study area varied from an average of 3.76 m in winter to an average of 5.09 m in summer during the year 2012, while in the year 2013, the depth to water level in the dug wells varied from an average value of 3.6 m in winter to an average value of 6.2 m in summer. The status of the bore wells as inferred from interaction with local farmers indicates that the bore wells have limited depth not exceeding 76 m. These bore wells essentially tap the fractured basaltic aquifer. The detailed bore well logs are not available from the area.

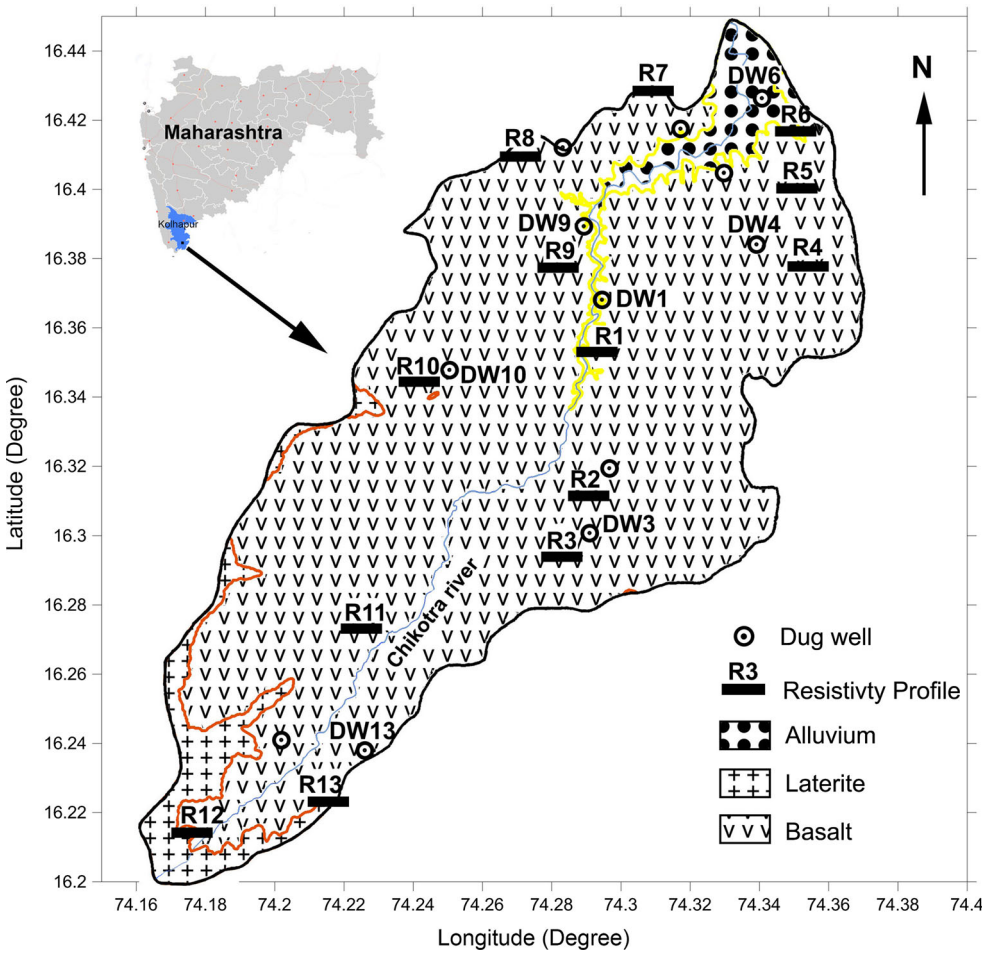

Fig. 2 Geological map of the study area showing the location of electrical resistivity imaging profiles as well as the dug wells

However, the dug wells in the area are productive and yielding water. Litho log data obtained from 12 dug wells in the study area reflected that in general the top section at 9 litho logs consists of alluvium/laterite/black cotton soil. Two litho logs showed volcanic breccias with red bole matrix as the top layer, whereas one litho log delineated partly weathered compact basalt as the top layer. The geological map of Chikotra basin along with resistivity profile locations are shown in Fig. 2.

Litho logs of some selected dug wells will be discussed in detail along with the resistivity models in "Interpretation and results". The hydro-geological section of the study area derived from the available dug well lithology is shown in Fig. 3.

Electrical resistivity imaging technique

The electrical resistivity method consists of measuring the potential at the surface, which results from a known current flowing into the ground (Bhattacharya and Patra 1968; VanNorstrand and Cook 1966; Ritz et al. 1999). A pair of current electrodes, A and B, and a pair of potential electrodes, M and N, is used. The apparent resistivity (ρ_a) is given by.

$$\rho_a = K\Delta V/I,$$

where K denotes a geometric coefficient dependent upon the electrode array, ΔV denotes the measured potential difference and I denotes the current intensity.

The ERI technique consists of using a multi-core cable with as many electrodes plugged into the ground at specific spacing, according to a sequence of readings predefined and stored in the internal memory of the equipment. The various combinations of transmitting (A, B) and receiving (M, N) pairs of electrodes construct the mixed sounding/profiling section, with a maximum investigation depth that mainly depends on the total length of the cable.

In electrical methods, the spatial resolution and depth of investigation is linked to the distance between electrodes. In a first approximation, for Schlumberger and Wenner arrays, the maximum depth of investigation is of the order of 20 % of the total length of the cable and the total length of the resistivity profile. This depth is reached for the

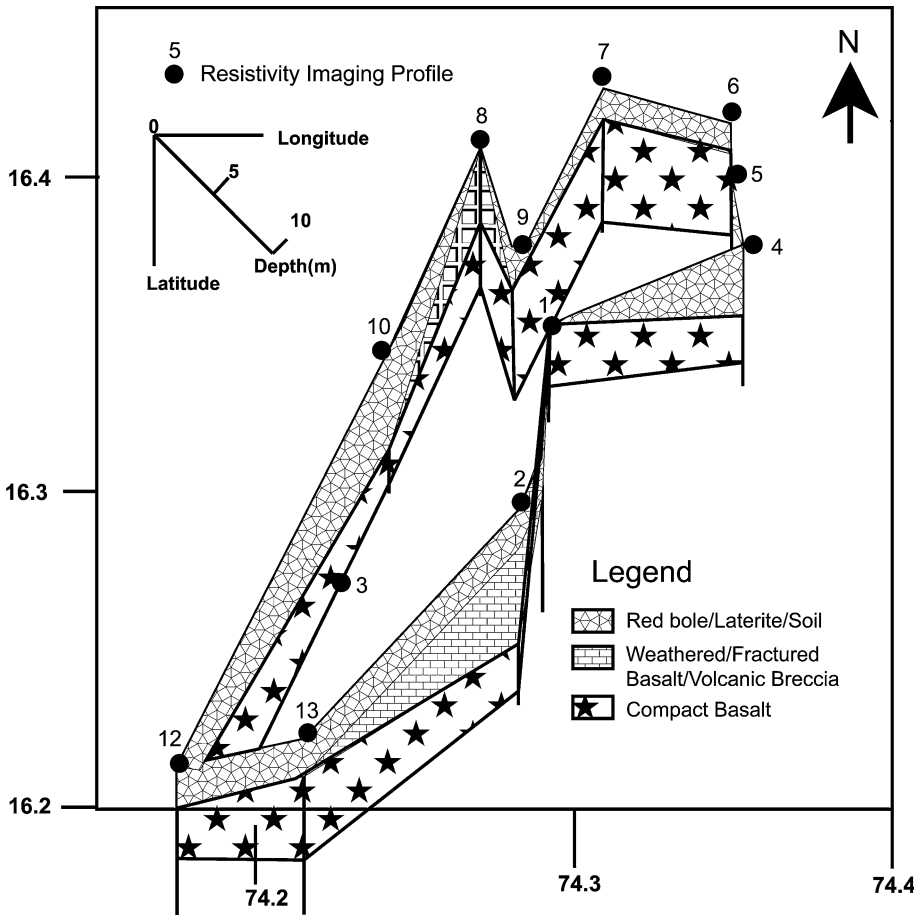

Fig. 3 Fence diagram showing the hydrogeological cross section of the study area

combination of the two extreme left and the two extreme right electrodes of the profile, and in the measuring report, plotting point corresponds to the bottom angle of the triangle of the pseudo section (Loke 2012). Nonetheless, Dahlin and Zhou (2004) are of the view that the precise resolution and penetration depth of arrays also depends on the electrical properties, anomalous features and the noise contamination levels, all of which may be simulated by numerical approaches.

Various types of electrode configuration can be used in ERI method. In the present case, data acquisition was performed using Wenner–Schlumberger configuration, a hybrid between Wenner and Schlumberger arrays (Pazdirek and Blaha 1996) with a constant inter-electrode spacing of 5 m. This array is moderately sensitive to both horizontal and vertical geological structures. The average investigation depth is greater than the Wenner array and the intensity of the signal is weaker than that of Wenner array but greater than that of dipole–dipole array and twice that of pole–dipole array, resulting in a higher signal-to-noise ratio (Dahlin and Zhou 2004). The horizontal data coverage is somewhat wider than the Wenner arrangement, but narrower than that achieved using dipole–dipole array (Loke 2012). Electrical resistivity imaging survey was carried out at 13 stations using IRIS make SYSCAL R1plus switch 48 system with 5 m inter-electrode separation. The maximum length of the profile was 235 m which resulted in a depth of investigation of about 50 m. The length of the profiles surveyed depends on the availability of free stretch land. As the top layer in the study area is dry and hard, the electrical coupling of the electrodes with the subsurface was enhanced by adding water dissolved with salt to each electrode, so as to minimize the contact resistance between the electrodes and the earth. The contact resistance was checked before data acquisition and was kept below 2 KΩ (Zarroca et al. 2014).

Data processing and inversion

The acquired apparent resistivity datasets were tomographically inverted to obtain true electrical resistivity distribution of the study area using the "RES2DINV" finite-difference software, based on the smoothness-constrained least squares inversion by a quasi-Newton optimization method (Loke and Barker 1996). An initial 2D

electrical resistivity model is generated, from which a response is calculated and compared to the measured apparent resistivity values of the field data. The optimization method then attunes the resistivity value of the model block iteratively until the calculated apparent resistivity values of the model are in close agreement with the measured values of the field data. The absolute error provides a measure of the differences between the model response and the measured data which is an indication of the quality of the model obtained. Using this scheme, 2D inverted models of true resistivity variation of sub-surface geological formations for all the 13 sites have been computed.

The RES2DINV software offers two inversion options-robust inversion (Loke et al. 2003) and smoothness-constrained least squares inversion (Loke and Dahlin 2002). It has been reported by Dahlin and Zhou (2004) that the robust inversion is better than the smoothness-constrained least squares inversion. In situations where the subsurface geology comprises a number of almost homogeneous regions but with sharp boundaries between different regions, the robust inversion scheme attempts to find a model that minimizes absolute changes in the model resistivity values (also known as L1 norm or blocky inversion method), thereby giving appreciably superior results. The smoothness-constrained optimization method (also known as L2 norm) on the other hand tries to minimize the squares of the spatial changes (or roughness) of the model resistivity values and tends to construct a model with a smooth variation of resistivity values. This approach is used only if the subsurface resistivity varies in a smooth or gradational manner.

In the present study, the 2D inversion of the field data along the 13 Wenner–Schlumberger profiles was carried out using the robust (L1 norm) inversion approach. The area surveyed is more or less flat and thus elevation correction was not included in the measurements. As the survey area was anticipated to be infested with urban noise, the robust inversion scheme was applied to the model resistivity values as well. The noisy data at a few sites were automatically filtered by removing the resistivity records having negative resistivity values or with a standard variation coefficient over 1 %. The convergence between the measured and calculated data was achieved after 7–12 iterations. The absolute error in the inverted models were below 5 % except at three profiles (absolute error values 6.5, 8.3 and 8.8 %) which appears to be rather noisy even after exterminating bad data points and increasing the damping factor. To reduce the distortion caused by the large resistivity variations near the ground surface and to obtain significantly better results, an inversion model with a cell width of half the unit electrode spacing was used for all the 13 imaging profiles (Loke 2012). These stations have been grouped into four zones for the sake of discussion. Site numbers 4, 5, 6 fall in the north-eastern part of the Chikotra basin, whereas sites 7, 8 and 9 are in the north-western part. The northern region of the basin is the downstream part of Chikotra River. The central part of the basin occupies sites 1, 2, 3 and 10 while the southern part comprises sties 11, 12 and 13, which is the upstream part of Chikotra River. All the imaging profiles are E–W oriented (Fig. 2).

Interpretation and results

The interpretation of the 2D resistivity models of 13 ERI profiles has been carried out to ascertain groundwater potential zones in Chikotra basin in view of the hydrogeological scenario. A generalized resistivity ranges for different litho units vis-à-vis water-bearing zones in the Deccan basalts (after Rai et al. 2013) is given in Table 1 below.

Deccan Trap Basalt forms an important water-bearing formation of the Chikotra basin. The nature of vesicular and massive basaltic unit of different lava flows has given rise to multi-layered aquifer system. The water-bearing capacity of vesicular basalt mostly depends upon size and shape of vesicles, density of vesicles and the degree of inter connection of vesicles. Massive basalt generally possesses negligible primary porosity or permeability and thus acts as an impermeable zone. However, due to fractures, joints and weathering of massive basalt at places, reasonably permeable structure is developed, which can be observed in open dug well section in the study area. In basaltic terrain, groundwater generally occurs under water table conditions in shallow aquifer and semi-confined to confined conditions in deeper aquifer. The groundwater here is alkaline in nature and is mostly Ca-HCO_3 type. However, detailed water chemistry data are not available in the study area.

ERI Profiles R4, R5 and R6

Site R4 belongs to Arjuni village, R5 belongs to Gaikwadi village, while R6 belongs to Kodni village in the north-eastern part of the study area (Fig. 2). The 2D resistivity

Table 1 Resistivity values for different litho units in Deccan Traps

Litho units	Resistivity range (Ωm)
Alluvial, black cotton soil, bole beds	5–10
Weathered/fractured vesicular basalt saturated with water	20–40
Moderately weathered/fractured vesicular basalt saturated with water	40–70
Massive basalt	>70

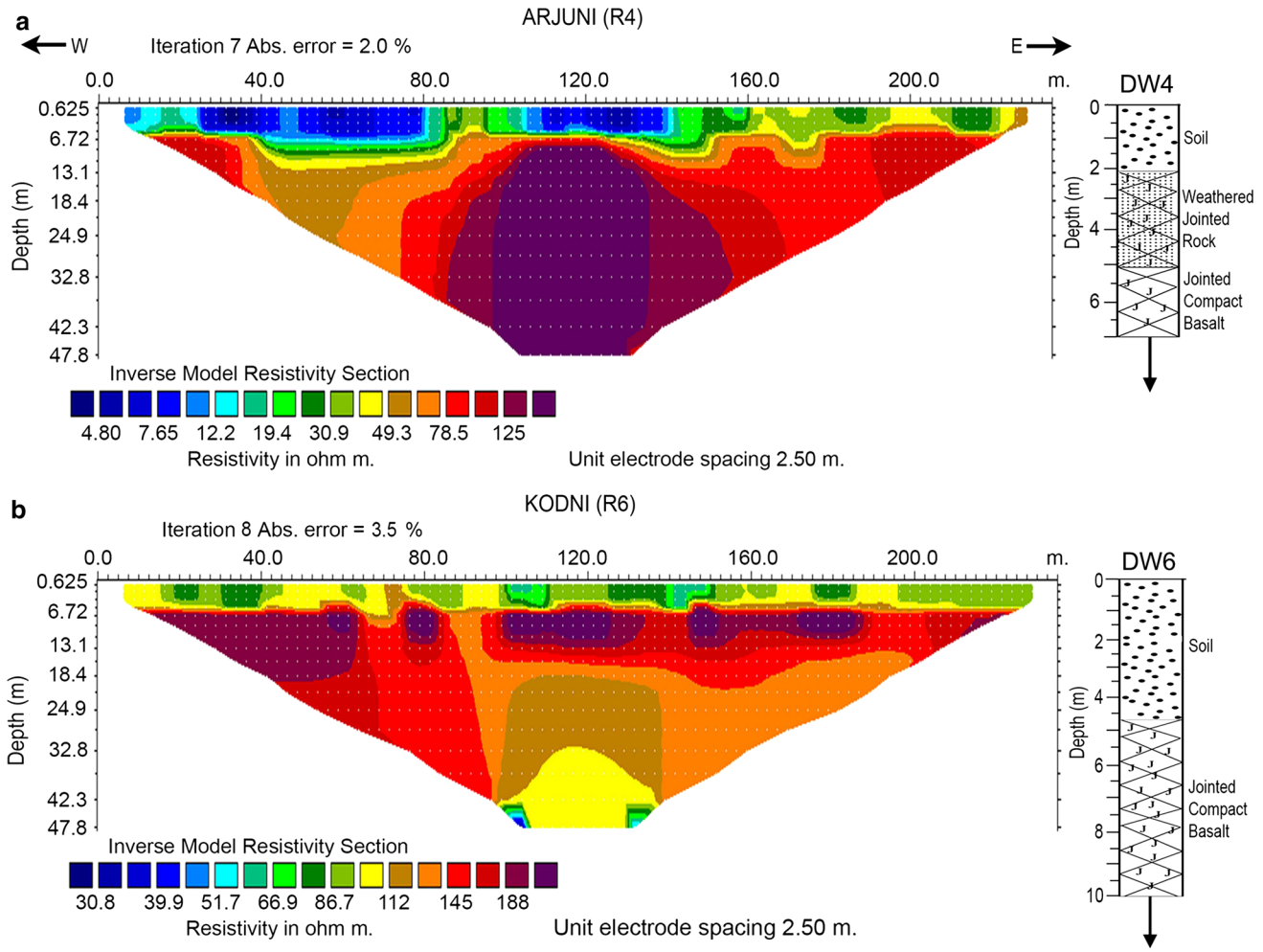

Fig. 4 **a** Inverted resistivity model of profile R4 (using Wenner–Schlumberger configuration) in west–east direction. The resistivity model is obtained using L1 norm (robust inversion method) with an electrode spacing of 2.5 m, iteration 7 and ABS error 2.0 %. The top 7–10 m consists of alluvium/weathered formation saturated with water followed by fractured basalt and massive basalt. The average sensitivity of the model is 1.232. Also shown is the dug well lithology (DW4) depicting top layer soil followed by weathered jointed rock and jointed compact basalt. **b** Inverted resistivity model of profile R6 (using Wenner–Schlumberger configuration) in west–east direction. The resistivity model is obtained using L1 norm (robust inversion method) with an electrode spacing of 2.5 m, iteration 8 and ABS error 3.5 %. The top 6 m consists of alluvium intercepted by jointed rock followed by compact basalt. Also shown is the dug well lithology (DW6) indicating top layer soil up to 5 m underlain by jointed compact basalt

inversion model sections for the sites R4, R5 and R6 are shown in Figs. 4a, b and 5.

Inverted resistivity model for R4 (Fig. 4a) suggests that the top layer is 7–10 m thick consisting of alluvium/weathered formation saturated with water having a resistivity of about 10–40 Ωm. This layer is underlain by a very thin layer of fractured basalt (45–70 Ωm) throughout the profile. However, at lateral distance between 40 and 70 m, this zone is extending down. This zone which is bounded by high-resistivity bodies (80–120 Ωm) on either side is likely being vertically recharged down to depths of about 33 m. A thick high-resistivity feature (>100 Ωm) is delineated at depth of 12 m between lateral distances 80–160 m which extends beyond the depth of study (45 m). This feature lies at the center of the profile, which is a rather high sensitive zone of the Wenner–Schlumberger array. The model sensitivity section indicates high values of sensitivity near the surface (up to depths of about 10 m) with decreasing values with depth. The average sensitivity of the model is estimated to be 1.232. The eastern part beyond 160 m distance is characterized by high resistivity (80–120 Ωm) below depths of 7 m. The dug well litho section (DW4) at Arjuni (Fig. 4a), which is at a distance of about 3 km from the imaging profile, suggests that the top 2 m comprises black cotton soil followed by weathered jointed fractured basalt up to about 5.2 m below which a thin layer of red bole seems to have developed and the bottom layer is the compact basalt

(resistivity value of >70 Ωm). The depth of the well is only 7 m. The water table in the year 2012 was 6.0 and 3.8 m during summer and winter season, respectively, whereas in the year 2013, the water table recorded was 6.5 m during summer and 1.85 m during winter. Being far away from the imaging profile, no quantitative conclusion can be drawn from the litho log and the imaging model. However, there is some agreement between the thickness of the top layer and the layer of fractured basalt in both the lithology of the dug well as well as the inverted resistivity model.

The resistivity model for profile R6 (Fig. 4b) indicate that the top 0–6 m is dry alluvium intercepted by jointed rock throughout the profile length having resistivities between 60 and 110 Ωm. At depths below 6 m, the model depicts a horizontal layer of massive basalt along the entire length of the profile having resistivities of the order of 140–200 Ωm. Below the center of the profile at lateral distance 120 m, a moderately low resistivity zone is seen at depths of 21 m increasing to deeper depths up to depth of investigation, having resistivity value of about 100–120 Ωm. This feature suggests that a sub-horizontal layer exists between 21 and 33 m, which could be a probable groundwater zone at deeper levels. Further, it is interesting to note two low-resistivity (30–70 Ωm) anomalies at the bottom edges of this feature, which is indicative of the fact that this could be a possible aquifer zone beneath the Traps. The lithological section (DW6) observed at Kodni (Fig. 4b) shows the top 5 m to be black cotton soil followed by jointed basalt. This dug well is located at a distance of about 2 km from the imaging site and has a total depth of 10 m. The water table levels during summer and winter in 2012 are 3.1 and 2.9 m, respectively, while the water table during summer and winter for the year 2013 are 4.2 and 3 m, respectively. The thickness of

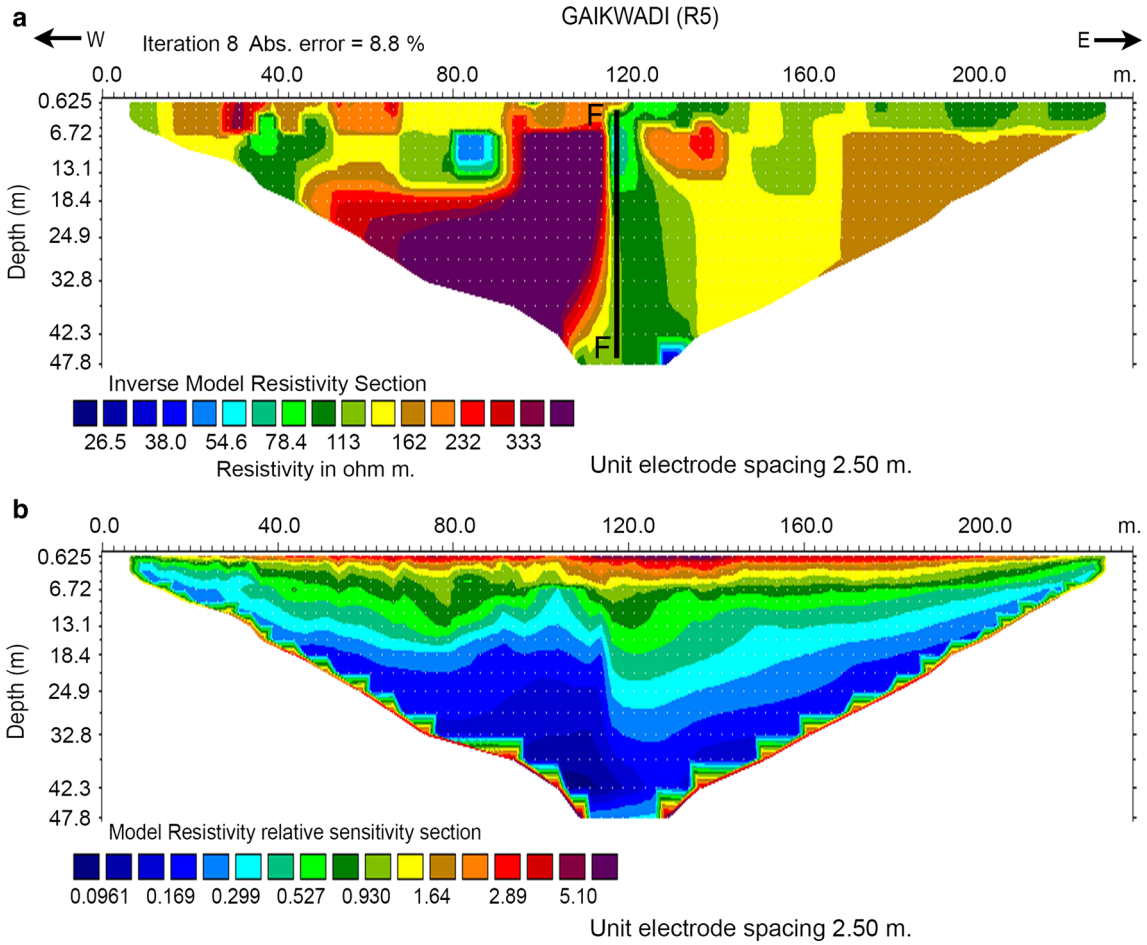

Fig. 5 **a** Inverted resistivity model of profile R5 (using Wenner–Schlumberger configuration) in west–east direction. The resistivity model is obtained using L1 norm (robust inversion method) with an electrode spacing of 2.5 m, iteration 8 and ABS error 8.8 %. The western part is very resistive representing massive basalt, while the eastern part is relatively conductive. A fault structure between resistive block and conductive zone at the center of the profile reveals prospective groundwater zone on the right side of the section. **b** Showing model resistivity relative sensitivity section of profile R5. The average model sensitivity is 1.04 while high value of sensitivity is observed up to depths of 13–25 m at the center of the profile where the fault zone is demarcated

the top 5 m in the lithology matches well with the thickness of the top layer in the inverted resistivity model, wherein black cotton soil has been delineated. The next layer in the litho log section depicts jointed basalt, which is also evident in the inverted resistivity model as high-to-moderate resistivity layers representing basalts.

The resistivity model for R5 (Fig. 5a) represents a heterogeneous image of the sub-surface litho units throughout the profile. On the western flank, the top layer up to depths of 6 m is characterized by high resistivities in the range of 140–300 Ωm. At lateral distance 40 m, a low-resistive zone (50–100 Ωm) is delineated from depths of 6 m extending downward. Further below lateral distance 80 m, another low-resistive block is identified having resistivities of the order of 50 Ωm at depths ranging from 7 to 15 m. The subsurface zone below 110 m is occupied by a high-resistive block from shallow depths up to the depth of investigation having resistivities in excess of 300 Ωm. This massive west dipping basaltic block seems to get wider at deeper levels. A linear low-resistivity zone is seen at the center of the profile extending upward from the deep to the shallow levels, which is indicative of the location of a fault. The massive basaltic block to the west is separated by this fault zone at 120 m lateral distance, beneath which lies a potential groundwater zone (40–100 Ωm) up to the depth of study. Further east, the top 6 m consists of soil/jointed weathered rocks having a resistivity of about 70–100 Ωm below which a homogeneous layer with resistivities of about 160 Ωm is delineated up to the depth of investigation. The resistivity model converged after eight iterations, however, high absolute error

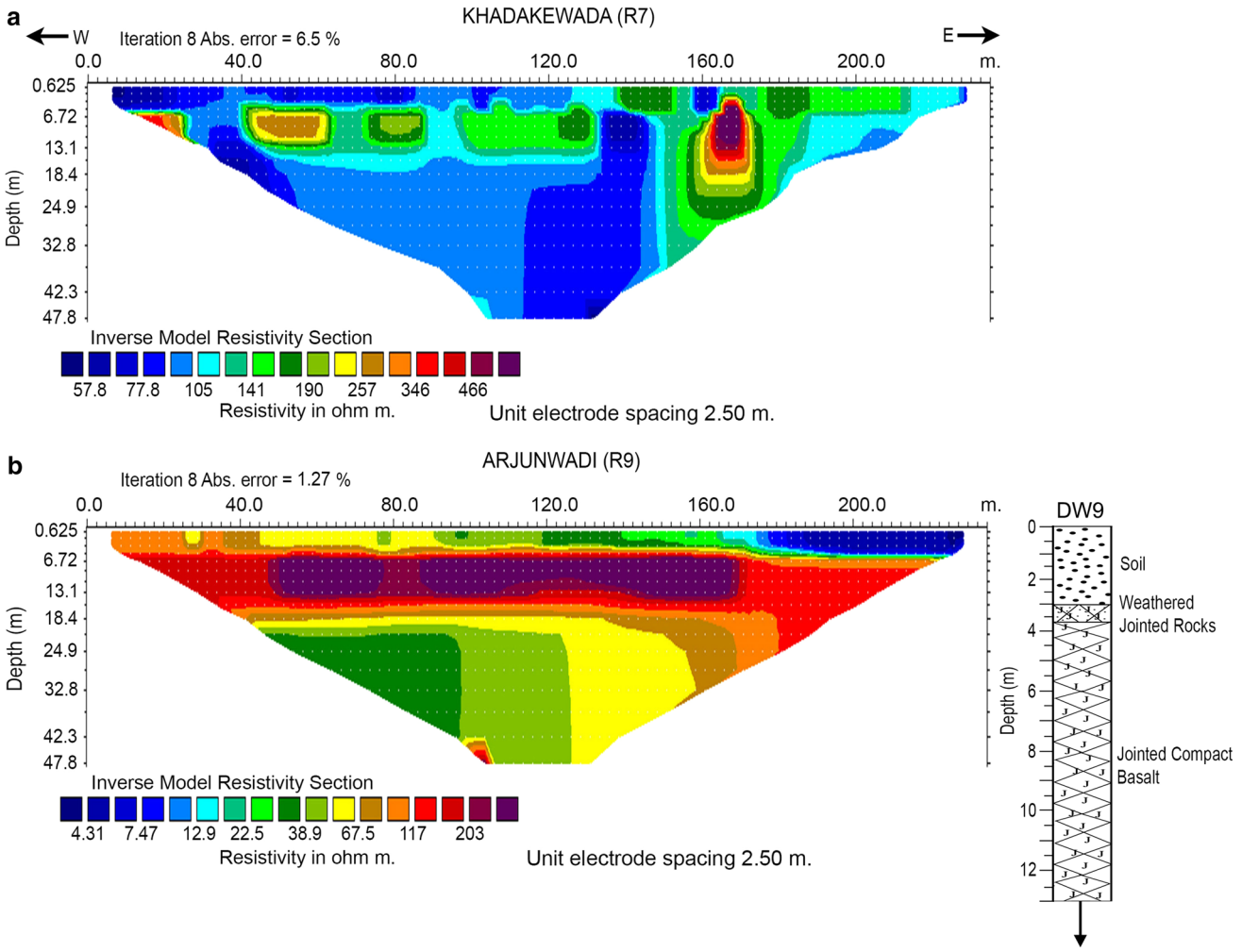

Fig. 6 **a** Inverted resistivity model of profile R7 (using Wenner–Schlumberger configuration) in west–east direction. The resistivity model is obtained using L1 norm (robust inversion method) with an electrode spacing of 2.5 m, iteration 8 and ABS error 6.5 %. The western part is characterized by jointed basalt below which low resistivity zone is observed, while the eastern part is occupied by massive basalts. **b** Inverted resistivity model of profile R9 (using Wenner–Schlumberger configuration) in west–east direction. The resistivity model is obtained using L1 norm (robust inversion method) with an electrode spacing of 2.5 m, iteration 8 and ABS error 1.27 %. Groundwater potential zone is observed at depths of about 21 m on the western part located beneath a basaltic layer. The average model sensitivity is 1.320. Also shown is the dug well lithology (DW9) indicating a 3 m thick top layer of soil below which a thin layer of weathered jointed rocks is revealed. Jointed compact basalt form the last unit of the dug well

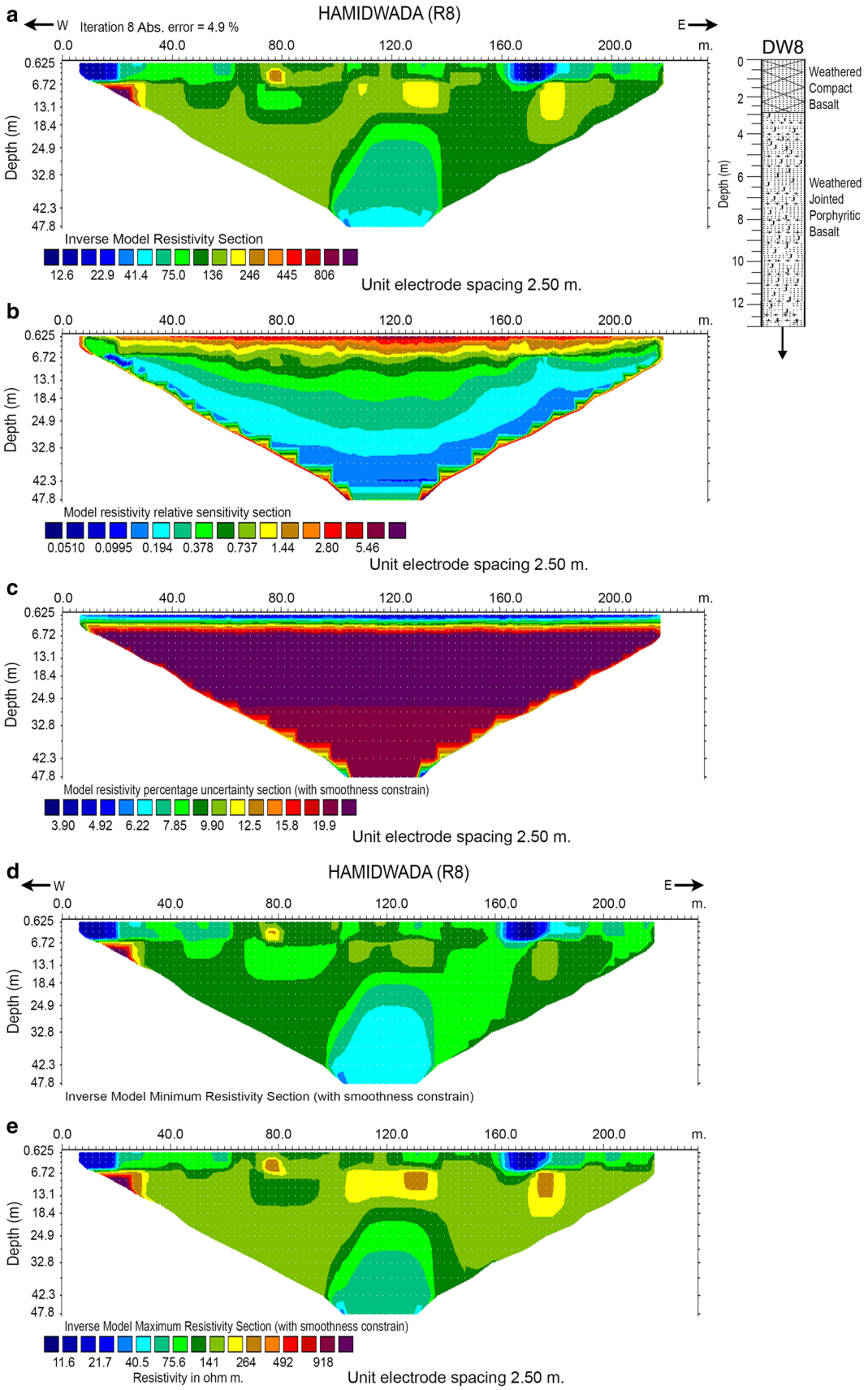
a
HAMIDWADA (R8)
W
Iteration 8 Abs. error = 4.9 %
E
0.0 40.0 80.0 120.0 160.0 200.0 m.
Depth (m)
0.625 6.72 13.1 18.4 24.9 32.8 42.3 47.8
Inverse Model Resistivity Section
12.6 22.9 41.4 75.0 136 246 445 806
Unit electrode spacing 2.50 m.
DW8
Depth (m)
0 2 4 6 8 10 12
Weathered Compact Basalt
Weathered Jointed Porphyritic Basalt
b
Model resistivity relative sensitivity section
0.0510 0.0995 0.194 0.378 0.737 1.44 2.80 5.46
Unit electrode spacing 2.50 m.
c
Model resistivity percentage uncertainty section (with smoothness constrain)
3.90 4.92 6.22 7.85 9.90 12.5 15.8 19.9
Unit electrode spacing 2.50 m.
d
HAMIDWADA (R8)
Inverse Model Minimum Resistivity Section (with smoothness constrain)
e
Inverse Model Maximum Resistivity Section (with smoothness constrain)
11.6 21.7 40.5 75.6 141 264 492 918
Resistivity in ohm m.
Unit electrode spacing 2.50 m.

◀**Fig. 7** **a** Inverted resistivity model of profile R8 (using Wenner–Schlumberger configuration) in west–east direction. The resistivity model is obtained using L1 norm (robust inversion method) with an electrode spacing of 2.5 m, iteration 8 and ABS error 4.9 %. A groundwater potential zone is observed at the center of the profile at depths of about 25 m. The dug well lithology (DW8) reveals a 1.5 m thick weathered basalt below which weathered jointed porphyritic basalt is seen. **b** Showing model resistivity relative sensitivity section of profile R8. The average model sensitivity is 1.231. Higher sensitivity values are observed at the top 10 m of the resistivity model which decreases with depth. **c** Model resistivity percentage uncertainty section of profile R8 in order to assess the accuracy of the inverted model. **d**, **e** Inverse model minimum and maximum resistivity section of profile R8. It can be observed that features common to both model sections can be considered more reliable. Two shallow minor low-resistive features are developed in the vicinity of lateral distance 10 and 170 m extending up to depth of 10 m from the surface having resistivity in the range of 10–20 Ωm. These two low-resistive features and the low-resistive aquifer zone at the center of the profile can be considered as conducive for groundwater prospecting

(8.8 %) was obtained due to laterally heterogeneous media. The inverted data were thus checked for sensitivity distribution wherein the minimum and maximum sensitivity was 0.08 and 10.4, respectively (Fig. 5b). The average model sensitivity was found to be 1.04 and high value of sensitivity was observed up to depths 13–25 m corresponding to the center of the profile where the fault zone was delineated (Fig. 5a). In a hard rock terrain, the electrolytic conduction is primarily responsible for current flow and thus the low resistivity is an indication of weathered, fractured zone saturated with water (Chandra et al. 2012) and therefore the highly sensitive region below lateral distance 120 m is an ideal aquifer zone.

ERI Profiles R7, R8 and R9

Profiles R7, R8 and R9 are located in Khadakewada, Hamidwada and Arjunwadi villages, respectively, in the northwestern part of the Chikotra basin (Fig. 2). The inverse resistivity models of these profiles have been shown in Figs. 6, 7. The resistivity model for R7 (Fig. 6a) exhibits that below a depth of 6–8 m, the sub-surface is divided into two different formations. The western part of the profile up to 140 m is characterized by jointed basalt up to about 17 m (resistivity ranging 100–150 Ωm) below which low-resistivity formation (50–90 Ωm) is observed, whereas the eastern part is occupied by massive basalts having resistivity values in excess of 180 Ωm up to depths of about 35 m. An aquifer zone is evident at 7 m depth continuing up to the depth of study at lateral distance 140 m. This aquifer is connected to the top layer by a fracture zone which appears to aid in recharging the aquifer. Another zone of weathered basalt saturated with water is observed at 40 m distance at depths of 8 m which is bounded by high-resistive bodies on either side. The western part of the profile between 10 and 20 m is characterized by a compact basaltic layer at 6 m depth. Similarly a 13 m thick compact basalt unit is seen at 160–170 m distance. Further east, potential aquifer zone is noticeable at 200 m distance at depths of about 13 m.

The inverse model resistivity section at R9 (Fig. 6b) delineated a 7-m top conductive layer between lateral distance 90–230 m having resistivities of the order 4–25 Ωm followed by a horizontal layer having thickness of about 15 m and resistivities in excess of 70 Ωm along the entire stretch of the profile with a root zone extending beneath 160 m distance. At depths beneath 21 m towards the western part between lateral distances 40–120 m, a groundwater potential zone (30–50 Ωm) is observed which extends up to the depth of investigation. This part which is located beneath the basaltic layer seems to be a prospective aquifer zone suitable for groundwater exploration. The average model sensitivity is calculated to be 1.320. The litho section (DW9) at Arjunwadi (Fig. 6b) which is at a distance of about 2 km from the imaging line depicts a 3 m thick top layer of black cotton soil, below which a thin layer of weathered jointed basalt is observed. The jointed compact basalt is underlying this thin layer up to depth of 13 m. The static water level of this well is 3 m in both summer and winter season for the year 2012, while it is 5.8 and 3 m for summer and winter, respectively, during the year 2013. The top conductive layer in the imaging section represents black cotton soil and the underlying resistive layer is indicative of weathered/jointed compact basalt, as inferred from the dug well litho section. The prospective groundwater zone delineated in the resistivity model is observed beneath the weathered/jointed compact basalt. It has been reported by Deolankar (1980) that the weathered basalt shows highest aggregate porosity (34 %) in DVP, whereas the specific yield is less (around 7 %). Though the porosity is high, the specific yield is very small signifying higher specific retention of the weathered basalt. This may be caused due to the presence of clay minerals in the weathered basalt which has higher water retention capacity.

The inverted model resistivity section at R8 (Fig. 7a) delineated an aquifer in the central part below lateral distance 120 m. This aquifer zone has a resistivity in the range of 30–70 Ωm at depths of 25 m and seems to become wider at deeper levels. The sensitivity function of the resistivity model has been accounted for wherein the minimum and maximum sensitivity was 0.0434 and 13.3 respectively, and the average sensitivity value obtained was 1.231. The inverse resistivity section converged after 8 iterations with absolute error of 4.9 %. The inverted resistivity model, the model resistivity sensitivity section, the model uncertainty values and the minimum and maximum resistivity values are given in Fig. 7a–e. It can be seen from Fig. 7b that higher sensitivity values are

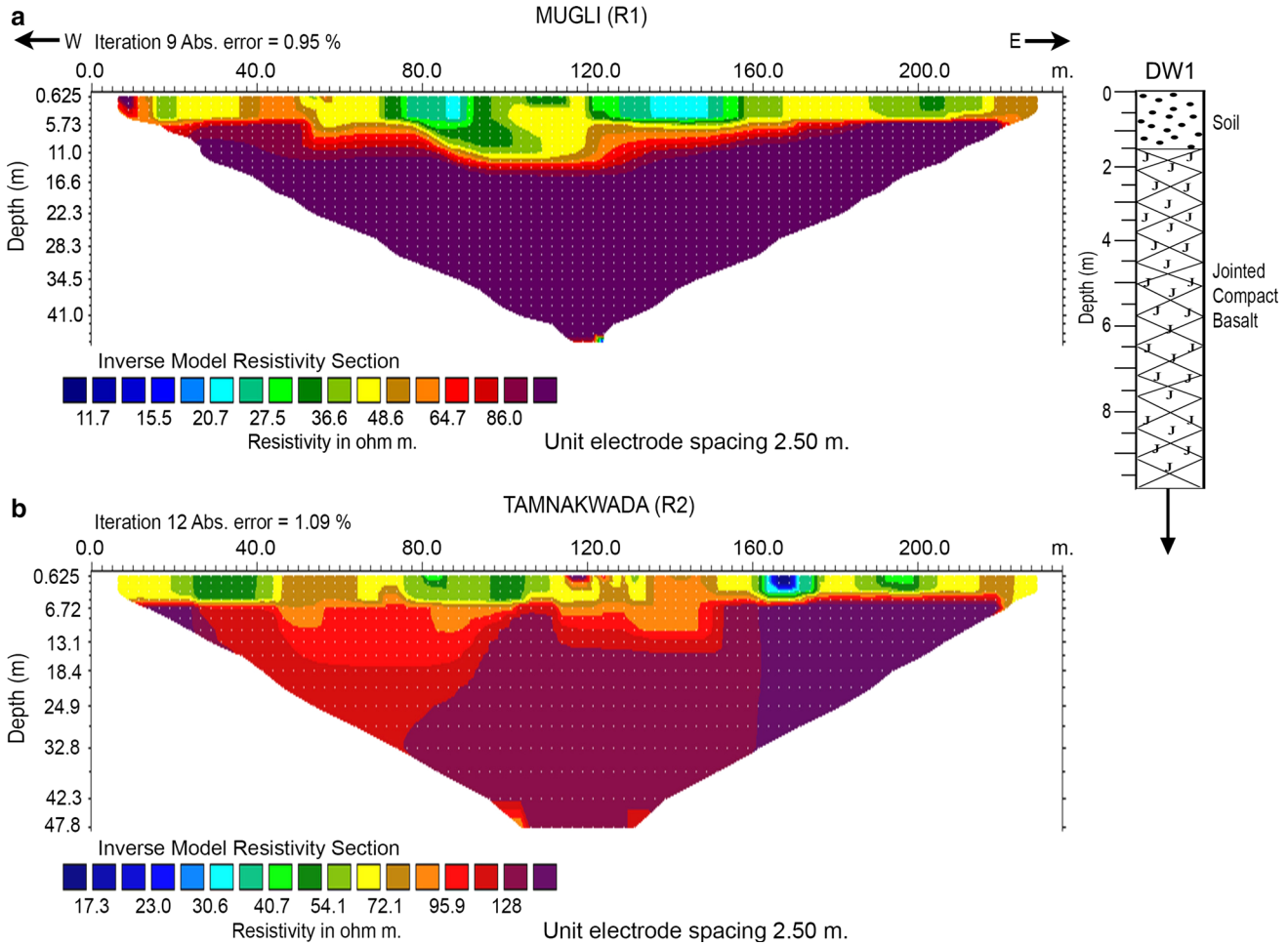

Fig. 8 **a** Inverted resistivity model of profile R1 (using Wenner–Schlumberger configuration) in west–east direction. The resistivity model is obtained using L1 norm (robust inversion method) with an electrode spacing of 2.5 m, iteration 9 and ABS error 0.95 %. The section reveals three low resistivity zones at 85 m, 140 m and 200 m distances with thickness varying from 5 to 10 m having resistivities of the order of 20–35 Ωm. This is underlain by a 10 m thick moderately resistive (~60–65 Ωm) layer, attributed to jointed basalt beneath which high-resistive formation is observed. Also shown is the dug well lithology (DW1) indicating a 1.5 m thick top layer of soil below which jointed basalt is revealed. **b** Inverted resistivity model of profile R2 (using Wenner–Schlumberger configuration) in west–east direction. The resistivity model is obtained using L1 norm (robust inversion method) with an electrode spacing of 2.5 m, iteration 12 and ABS error 1.09 %. The top 6 m is low resistive intercepted by patches of moderately resistive zones. A thick horizontal high resistivity (>100 Ωm) below 6 m and extending up to depth of investigation is due to compact basalt

observed at the top 10 m of the resistivity model which decreases with depth as the near-surface materials have a large influence on the measured apparent resistivity values. Figure 7c shows the model uncertainty values obtained in order to assess the accuracy of the inverted model. For estimating the uncertainty, smoothness constraint is included in the model, so that the model uncertainty values are less sensitive to the size of the model cells. The minimum and maximum resistivity values of each cell at the limits of the model uncertainty range are shown in Fig. 7d, e. It can be discerned from the figure that features common to both model sections can be considered more reliable. Two shallow minor low-resistive features are developed in the vicinity of lateral distance 10 and 170 m and extend up to depth of 10 m from the surface having resistivity in the range of 10–20 Ωm. These two low-resistive features and the low-resistive aquifer zone at the center of the profile reflect very well in Fig. 7d, e and thus can be considered as conducive for groundwater prospecting. The top and underlying layers at the central part of the profile is having resistivities of about 70–150 Ωm. These layers are perhaps devoid of alluvium and are characterized by weathered and jointed basalt. The lithological dug well section (DW8) at Hamidwada (Fig. 7a), which is about 200 m from the imaging profile, suggests that the top 1.5 m comprised weathered basalt below which weathered jointed porphyritic compact basalt is encountered. There is a fair degree of corroboration between the litho log and the resistivity section, at least up to the depth of the dug well (13 m). The static water level during the year 2012 is 4.8 and 3.2 m for

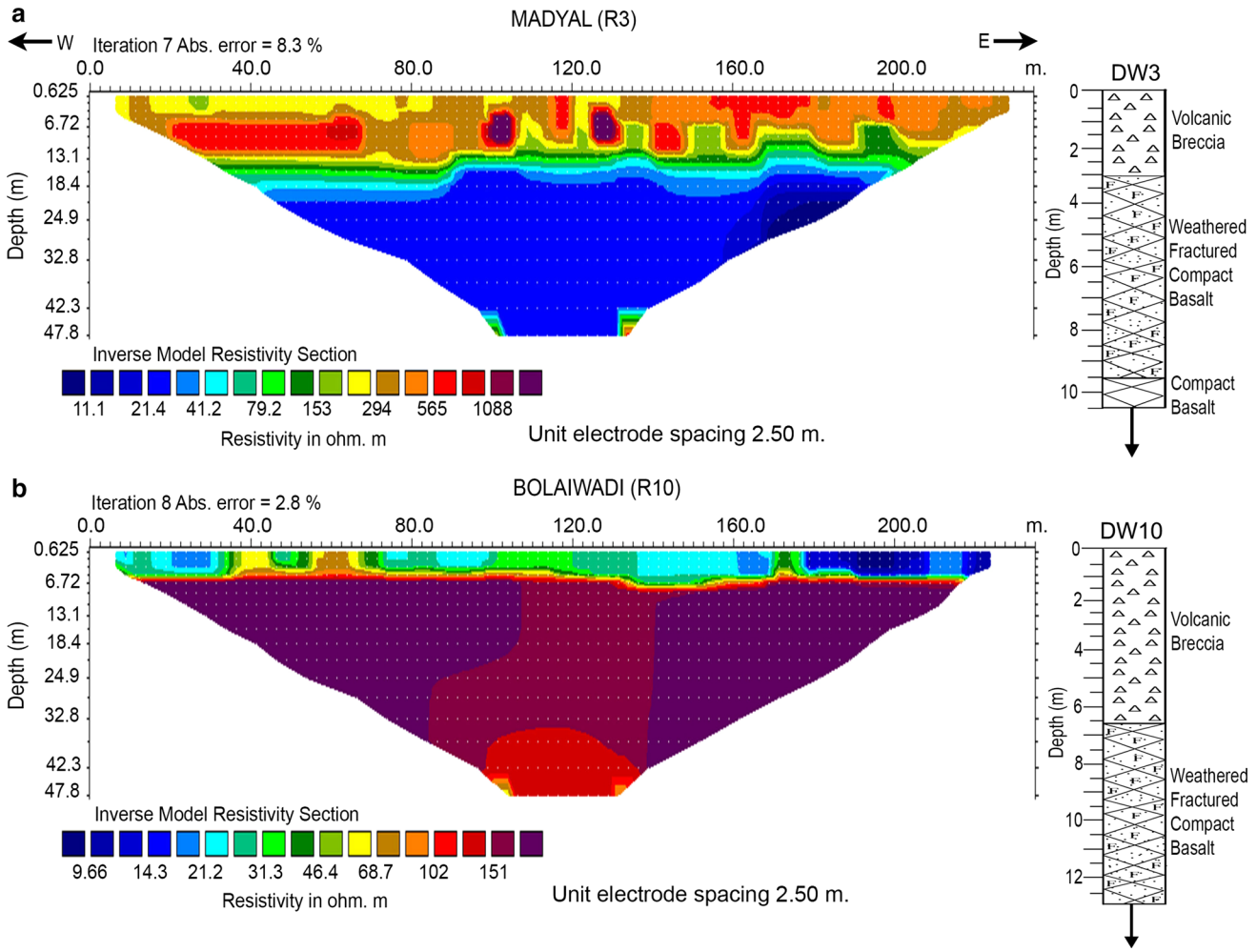

Fig. 9 **a** Inverted resistivity model of profile R3 (using Wenner–Schlumberger configuration) in west–east direction. The resistivity model is obtained using L1 norm (robust inversion method) with an electrode spacing of 2.5 m, iteration 7 and ABS error 8.3 %. The top 15 m is characterized by high resistivity (>160 Ωm) beneath which a 3 m thin horizontal layer is delineated having resistivity of about 45–80 Ωm. Underlying this layer, a relatively low-resistive (about 20 Ωm) layer is observed at 18 m depth extending up to the depth of study. Vertical anomalies and inversion artifacts characteristic of fracture zone is observed at the center of the profile just above the low resistivity layer. The lithological section (DW3) shows that the top 3.2 m comprises volcanic breccias followed by a 6.5 m thick layer of weathered and fractured basalt. The last unit here is the compact basalt. **b** Inverted resistivity model of profile R10 (using Wenner–Schlumberger configuration) in west–east direction. The resistivity model is obtained using L1 norm (robust inversion method) with an electrode spacing of 2.5 m, iteration 8 and ABS error 2.8 %. The top 6–7 m is conductive due to wet alluvium beneath which a thin moderately resistive layer is revealed. At the center of the profile a high-resistive anticlinal feature is observed at depths of about 35 m. At the two edges of this feature, low resistivity zones seem to develop. No promising aquifer zones are seen at this profile up to the probing depths. The lithological section (DW10) shows that the top 6.7 m comprises volcanic breccias followed by weathered and fractured basalt up to 13 m

summer and winter, respectively. Static water levels of 5.7 and 3.5 m for summer and winter seasons, respectively, was obtained for the year 2013. Due to limited depth of the dug well, the aquifer zone delineated in the inverted resistivity model beneath the weathered jointed basalt at depths of 25 m could not be confirmed.

ERI Profiles R1, R2, R3 and R10

Profiles R1 (Mugli), R2 (Tamnakwada), R3 (Madyal) and R10 (Bolaiwadi) are located in the central part of the Chikotra basin. The inverted resistivity models are shown in Figs. 8 and 9. Imaging section at R1 reveals three low resistivity zones at 85, 140 and 200 m distances (Fig. 8a). The thickness of these zones varies from 5 to 10 m having resistivities of the order of 20–35 Ωm. This is underlain by a thin (about 10 m) moderately resistive (~60–65 Ωm) layer, attributed to jointed basalt. Below this layer, high-resistive formation (>85 Ωm) is encountered throughout the profile up to depths of investigation. The inverted model converged after 9 iterations with absolute error of 0.95 %. The lithological section (DW1) at Mugli (at a

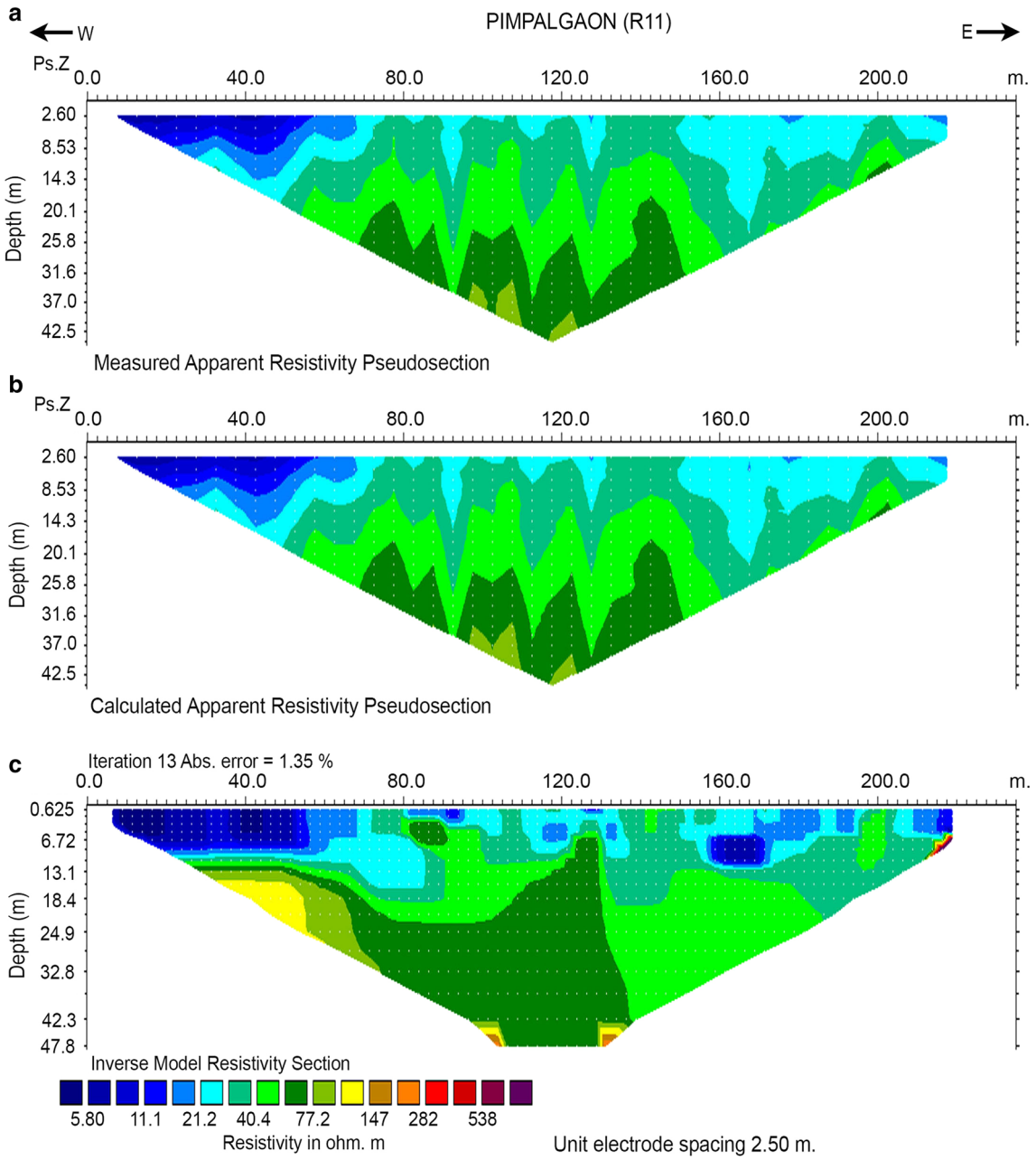

Fig. 10 **a** Measured apparent resistivity pseudo section of profile R11. **b** Calculated apparent resistivity pseudo section of profile R11. **c** Inverted resistivity model of profile R11 (using Wenner–Schlumberger configuration) in west–east direction. The resistivity model is obtained using L1 norm (robust inversion method) with an electrode spacing of 2.5 m, iteration 13 and ABS error 1.35 %. The top layer is conductive due to alluvium. A small low-resistive zone below lateral distance 160 m at depth of about 8 m appears to be a potential aquifer. The deeper layers are resistive and can be attributed to massive basalts

distance of about 800 m from the imaging profile) suggests that the dug well comprised a 1.5-m-thick layer of soil followed by jointed basalt up to depths of 10 m (Fig. 8a). The low-resistive zone and the underlying moderately resistive zone observed in the resistivity model can thus be attributed to soil and jointed basalt. The dug well is only 10 m deep. The static water levels of the dug well are measured as 0.15 m during summer and winter for the year 2012. These values are 4.6 and 0.6 m for summer and winter, respectively, during the year 2013. It is pertinent to mention here that Chikotra River is flowing in vicinity to the west of this dug well as well as the resistivity profile. Perhaps the very shallow static water levels observed are due to the influence of the river.

The inverted resistivity model at R2 (Fig. 8b) is almost similar to that of R1. The model indicates the top layer to be 6 m thick comprising low-resistivity pockets intercepted by patches of moderately resistive zones. The low

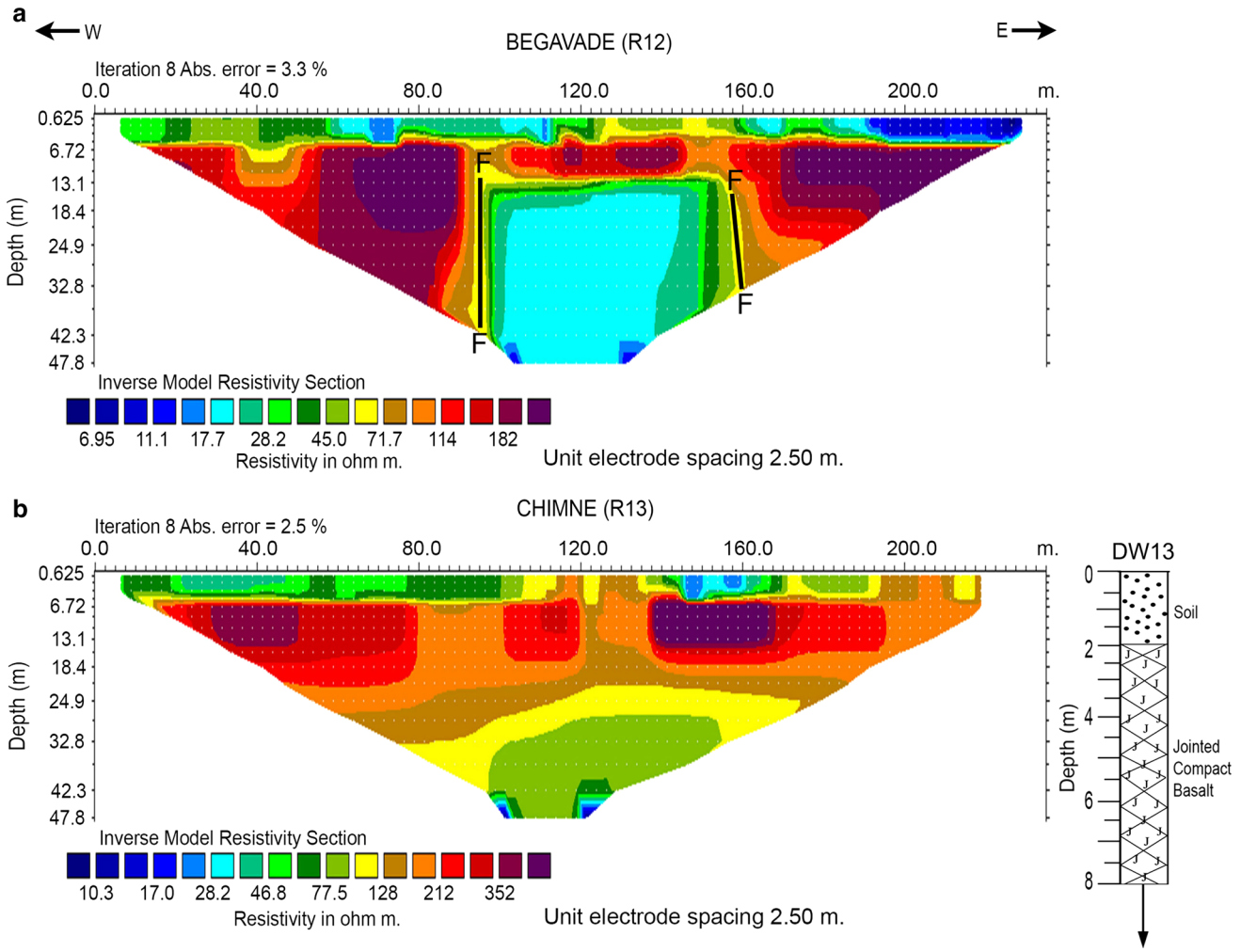

Fig. 11 **a** Inverted resistivity model of profile R12 (using Wenner–Schlumberger configuration) in west–east direction. The resistivity model is obtained using L1 norm (robust inversion method) with an electrode spacing of 2.5 m, iteration 8 and ABS error 3.3 %. The image reveals a broad aquifer zone (resistivity of 15–50 Ωm) located between 100 and 150 m in the central part of the profile extending downward beyond the depth of study (47 m) and is bounded by two vertical blocks of high-resistive massive basalt on either side. This aquifer body is lying beneath a horizontal layer of massive basalt at depths of 13 m. Two fault zones with surface projection at 100 and 150 m separates this aquifer body from the massive basalts. **b** Inverted resistivity model of profile R13 (using Wenner–Schlumberger configuration) in west–east direction. The resistivity model is obtained using L1 norm (robust inversion method) with an electrode spacing of 2.5 m, iteration 8 and ABS error 2.5 %. The model suggests a high-resistive (>150 Ωm) thick horizontal layer delineated up to depths of 25 m along the entire length of the profile. A groundwater prospective zone with resistivity values of 30–60 Ωm is observed at 30 m depth at the center of the profile which extends up to the bottom depth of 47.8 m. This zone is being vertically recharged. The lithological section (DW13) at Chimne delineated about 2 m thick layer of lateritic soil at the top below which jointed basalt is seen up to depth of 8 m which is indicative of potential groundwater aquifer zones in the jointed basalt and beyond

resistivity in the range of 20–50 Ωm is observed at 20–40, 80–110, 160–175 and 185–205 m distance over the profile. The moderate resistivity zone has a resistivity value of about 60 Ωm. The bottom-most layer in the model below 6 m depicts a thick horizontal high-resistivity layer with values in excess of 100 Ωm extending up to the depth of study, which could be the compact basalt.

The imaging section at R3 (Fig. 9a) suggests that the top 15 m is characterized by high resistivity (>160 Ωm) throughout the lateral distance of the profile. Below this, a 3-m thin horizontal layer is delineated having resistivity of about 45–80 Ωm. Underlying this layer, a relatively low-resistive (about 20 Ωm) layer is observed at 18 m depth extending up to the depth of study. At the center of the profile (120 m distance), vertical anomalies and inversion artifacts characteristic of fracture zone is observed just above the low resistivity layer. The lithological section (DW3) at village Madyal (Fig. 9a), which is at a distance of about 200 m from the resistivity profile, shows that the top 3.2 m comprises volcanic breccias followed by a 6.5-m-thick layer of weathered and fractured basalt. The last unit here is the compact basalt. The litho log section at

Madyal (Fig. 9a) broadly matches with the resistivity section (R3) wherein the top layer is resistive which can be attributed to the volcanic breccias. Volcanic breccias comprise blocks of lava in an ash matrix and are the product of an explosive eruption. The second and third layer in the inverted model can be considered as weathered fractured and compact basalt. The dug well litho log is up to a depth of only 10.5 m and thus the low-resistivity zone at depths of about 18 m depicted in the resistivity model could not be accounted for. The static water levels observed here are 9.7 and 9 m during summer and winter, respectively, for the year 2012. During the year 2013, these values are 10 and 9.2 m for summer and winter season, respectively. The water table here is at a deeper level presumably due to the top layer volcanic breccias. The resistivity model also suggests that the low-resistive layer is at a depth of about 18 m.

The inverted resistivity model at R10 (Fig. 9b) indicates that the top 6–7 m is conductive (resistivity of about 10–50 Ωm) throughout the profile length. This is due to the wet alluvium zone. Below this, a thin moderately resistive (80–100 Ωm) layer is delineated throughout the profile length. Below lateral distance 110–140 m, a high-resistivity (about 150 Ωm) feature is seen at depths of 7 m extending up to the depth of study. On either side of this feature the sub-surface is highly resistive (in excess of 150 Ωm). These could be attributed to massive basalts. At lateral distance 120 m, an anticlinal body with resistivities of the order of 110 Ωm is deciphered at depth of about 35 m. At the two edges of this body small lobes of low resistivity (60–70 Ωm) seems to develop. However, there are no signatures of aquifer zones being developed at this profile at least up to the penetrating limits of investigation. The dug well lithological section (DW10) (about 200 m from the imaging profile) derived at Bolaiwadi (Fig. 9b) suggests that the top 6.7 m is infested with volcanic breccia followed by weathered fractured basalt up to 13 m, which is comparable to the inverted resistivity model. The static water levels as observed in this dug well are 8.2 and 6 m during summer and winter, respectively, for the year 2012, while these values are 9 and 5.4 m for summer and winter, respectively, during the year 2013.

ERI Profiles R11, R12 and R13

The imaging stations R11 (Pimpalgaon), R12 (Begavade) and R13 (Chimne) are located at the southern portion of Chikotra basin which is the upstream part of the Chikotra River. The inverted resistivity models are shown in Figs. 10 and 11. The measured and calculated apparent resistivity pseudo sections along with the inverted resistivity model for profile R11 are shown in Fig. 10a–c. The inverted model at imaging site R11 (Fig. 10c) shows low-resistive (5–20 Ωm) alluvial deposits up to depth of 11 m from lateral distances 10–70 m. At rest of the profile, the resistivity varies from 10 to 60 Ωm up to depths of 15 m. The small low-resistive zone below lateral distance 160 m at depth of about 8 m appears to be a potential aquifer. On the western part, at depth of 15 m between lateral distances 30–70 m, a high-resistive (up to 120 Ωm) layer is seen. Below 15 m at rest of the profile, the sub-surface is characterized by resistivities of the order of 30–70 Ωm indicative of weathered fractured basalt. Two small lobes of very high resistivity (120–200 Ωm) is visible at the edges (100 and 130 m, respectively) at depths of 47 m, which could be attributed to massive basalts at these depths.

The resistivity model for imaging profile R12 (Fig. 11a) indicates a broad aquifer zone bounded by two vertical blocks of high-resistive massive basalt on either side. This aquifer zone is located between 100 and 150 m in the central part of the profile which extends downward beyond the depth of study (47 m). This aquifer body has a resistivity in the range of 15–50 Ωm and is lying beneath a horizontal layer of massive basalt at depths of 13 m. Two fault zones with surface projection at 100 and 150 m separates this aquifer body from the massive basalts. This zone is being vertically recharged (Fig. 11a) and appears to be excellent for groundwater exploration.

The resistivity model of R13 (Fig. 11b) suggests a high-resistive thick horizontal layer delineated up to depths of 25 m having resistivities greater than 150 Ωm along the entire length of the profile. A groundwater prospective zone with resistivity values of 30–60 Ωm is observed at 30 m depth at the center of the profile which extends up to the bottom depth of 47.8 m. This zone is also being vertically recharged. Two small low-resistive features are seen at the edges at 100 and 120 m distance at depths of 47 m, which further suggests that this zone is saturated and containing clay, though the present study limits to depth of 47 m. The lithological section (DW13) at Chimne (Fig. 11b), located at about 2 km away from the imaging profile, delineated about 2-m-thick layer of lateritic soil at the top below which jointed basalt is seen up to depth of 8 m which is indicative of the fact that potential groundwater aquifer zones could be present in the jointed basalt and beyond. This dug well with a depth of 8 m recorded static water levels of 2.2 and 2 m in summer and winter, respectively, during 2012 and 2.6 and 2.2 m in summer and winter seasons, respectively, for the year 2013.

Discussions

The resistivity models obtained after inversion of measured apparent resistivity data at 13 profiles suggests that the subsurface structure is fragmented into multiple units due to

weathering, fracturing and faulting. The massive basaltic units are covered by a thin veneer of alluvium and weathered and jointed rocks formed by erosion and subsequent deposition, which form unconfined aquifer zones which are the main sources of groundwater to the dug wells in DVP. The lithology of the limited shallow dug wells available in the study region reveal that the top layer comprised volcanic breccias with red bole matrix and/or laterite or black soil followed by weathered/fractured basalts and compact basalts as bedrock. The low-resistive feature shows downward extension of resistivity decreasing with depth which appears to be linked with a fault zone extended to deeper levels beyond 47 m. It has been reported by Zhu et al. (2009) that if a low resistivity zone extends to near-surface terrain from the deep, only then it can be interpreted that the low-resistivity zone can be an indication of the location of fault zone.

The study demonstrated the efficacy of using electrical resistivity in imaging the sub-surface from which the underlying structures and extent of fractures and faults that influence the occurrence of groundwater in basaltic rocks can be evaluated, thus enhancing the accuracy of interpretation with minimum error. Resistivity models produced by inverse modeling of measured apparent resistivity data indicate prospective groundwater zones at several sites in the top layer which can be explored for groundwater. Likewise, resistivity models have further deciphered groundwater potential zones within and below traps in the hard rock terrain of Deccan volcanics. In general L1-based resistivity inversion results are stable and well correlated with the available geological information. Moreover, 2D resistivity model based on robust inversion appears to be appropriate to infer sharp lateral resistivity variation caused by multiple episodes of lava flows and genesis of hard rock terrain of DVP. It is worthwhile to note that L1-based inversion scheme is more robust than that of L2-based inversion scheme to take care of the uncontrolled error/outliers in the data, and hence provide some confidence to apply the algorithm for modeling the resistivity data. The reliability of the resistivity models of the subsurface formations is also validated by the litho log of the available dug wells in the study area. In addition to sharply mapping the detailed geological features such as faults, lineaments, fractures, etc., in the hard rock terrain, the present analysis also define the potential groundwater prospecting zones which is of considerable significance for groundwater exploration. Further these results are useful to gain better insights of the hydro-geological system of the study area.

Conclusions

In the present study, groundwater potential zones were investigated using electrical resistivity imaging (ERI) technique over Chikotra basin located in the hard rock terrain of DVP. The L1 norm-based robust inversion scheme has been used to infer the sharp resistivity changes laterally while the presence of the uncontrolled error in the data/outlier are taken into care by sound mathematical background of the robust inversion scheme. The inverted resistivity models are well correlated with the existing lithology. The main results are summarized as follows:

1. The top layer in the study area comprises red bole, laterite or black soil followed by weathered/fractured rock grading into compact basalts. The sources of groundwater appear to be available in weathered and fractured basalt trapped between weathered overburden and hard rock.
2. Results from the 2D inverted models of resistivity variation with depth suggest the occurrence of aquifers mostly in weathered/fractured zones within the traps or beneath it. Resistivity images at almost all the stations have delineated a wet zone in the top 5–7 m followed by weathered zone up to depths of about 30 m. These models have further delineated potential groundwater locales in the top layer as well as within and below the traps in the basin which can be targeted for groundwater exploration.
3. The present results also suggest that there is a potential aquifer zone in Gaikwadi village at depth of 47 m which could be targeted for groundwater exploration. The robust resistivity inversion indicates the presence of potential aquifers in the places of Kodni at depth 25 m. At Khadkewadi and Hamidwada, the aquifer depth lies in the range of 18–42 m.
4. The present robust inversion scheme is found to be useful to map the sharp changes of the resistivity distribution by utilizing L1-based robust inversion algorithm. The present results provide deep insights to define precisely the extension of aquifer in the hard rock terrain of India which is of considerable societal interest.

Acknowledgments The authors are grateful to Dr. D.S. Ramesh, Director, IIG, for according permission to publish this work. Thanks are also due to Prof. S.G. Gokarn for many fruitful discussions. The authors are grateful to Shri B.I. Panchal for drafting the figures. The authors are obliged to the anonymous reviewers for the excellent comments and suggestions for improving the manuscript. SM is thankful to Director, Indian School of Mines (ISM), Dhanbad for encouragement and motivation.

References

Bhattacharya PK, Patra HP (1968) Direct current geoelectric sounding, principles and interpretation, methods in geochemistry and geophysics, vol 9. Elsevier Publishing Company, Amsterdam 135p

Bose RN, Ramkrishna TS (1978) Electrical resistivity surveys for ground water in the Deccan trap country of Sangli district, Maharashtra. J Hydrol 38:209–221

Chandra S, Nagaiah E, Reddy DV, Ananda Rao V, Ahmed S (2012) Exploring deep potential aquifer in water scarce crystalline rocks. J Earth Syst Sci 121(6):1455–1468

Dahlin T (1996) 2D resistivity surveying for environmental and engineering applications. First Break 14:275–283

Dahlin T, Zhou B (2004) A numerical comparison of 2D resistivity imaging with ten electrode arrays. Geophys Prospect 52:379–398

Deolankar SB (1980) The Deccan Basalt of Maharashtra, India- their potential as aquifers. Groundwater 18(5):434–437

Devi SP, Srinivasulu S, Raju KK (2001) Delineation of groundwater potential zones and electrical resistivity studies for groundwater exploration. Environ Geol 40:1252–1264

Edet AE, Okereke CS (2001) A regional study of saltwater intrusion in southeastern Nigeria based on the analysis of geoelectrical and hydrochemical data. Environ Geol 40:1278–1289

El-Qady G, Ushijima K, El-Sayed A (2000) Delineation of a geothermal reservoir by 2D inversion of resistivity data at Hammam Faraun area, Sinai, Egypt. In: Proceeding of the World Geothermal Congress pp 1103–1108

Francese R, Mazzarini F, Bistacchi ALP, Morelli G, Pasquarè G, Praticelli N, Robain H, Wardell N, Zaja A (2009) A structural and geophysical approach to the study of fractured aquifers in the Scansano-Magliano in Toscanaridge, southern Tuscany, Italy. Hydrogeol J 17:1233–1246

Frohlich RK, Barosh PJ, Boving T (2008) Investigating changes of electrical characteristics of the saturated zone affected by hazardous organic waste. J Appl Geophys 64:25–36

Ghosh P, Sayeed MRG, Islam R, Hundekari SM (2006) Inter-basaltic clay (bole-bed) horizons from Deccan traps of India: implications for palaeo-climate during Deccan trap volcanism. Palaeogeog Palaeoclimatol Palaeoecol 242:90–109

Griffiths DH, Barker RD (1993) Two dimensional resistivity imaging and modeling in areas of complex geology. J Appl Geophys 29:211–226

Gupta G, Erram VC, Kumar S (2012) Temporal geoelectric behavior of dyke aquifers in northern Deccan Volcanic Province, India. J Earth System Sci 121(3):723–732

Hamzah U, Samudin AR, Malim EP (2007) Groundwater investigation in Kuala Selangor using vertical electric sounding (VES) surveys. Environ Geol 51:1349–1359

Hermans T, Vandenbohede A, Lebbe L, Martin R, Kemna A, Beaujean J, Nguyen F (2012) Imaging artificial salt water infiltration using electrical resistivity tomography constrained by geostatistical data. J Hydrol 438–439:168–180

Hodlur GK, Dhakate R, Andrade R (2006) Correlation of vertical electrical sounding and borehole-log data for delineation of saltwater and freshwater aquifers. Geophysics 71(1):G11–G20

Horton RE (1945) Erosional development of streams and their drainage basins: hydrophysical approach to quantitative morphology. Geol Soc America Bull 56:275–370

Karlik G, Kaya MA (2001) Investigation of groundwater contamination using electric and electromagnetic methods at an open waste-disposal site: a case study from Isparta, Turkey. Environ Geol 40:725–731

Keller GV, Frischknecht FC (1966) Electrical methods in geophysical prospecting. Pergamon Press Inc, Oxford

Koefoed O (1979) Geosounding principles 1: Resistivity sounding measurements. Elsevier Science Publishing Company, Amsterdam

Kumar D, Rao VA, Nagaiah E, Raju PK, Mallesh D, Ahmeduddin M, Ahmed S (2010) Integrated geophysical study to decipher potential groundwater and zeolite-bearing zones in Deccan Traps. Curr Sci 98(6):803–814

Kumar D, Thiagarajan S, Rai SN (2011) Deciphering Geothermal Resources in Deccan Trap Region using Electrical Resistivity Tomography Technique. J Geol Soc India 78:541–548

Kundu MC, Mandal B (2009) Assessment of potential hazards of fluoride contamination in drinking groundwater of an intensively cultivated district in West Bengal, India. Environ Monit Assess 152:97–103

Lenkey L, Hamori Z, Mihalffy P (2005) Investigating the hydrogeology of a water supply area using direct-current vertical electrical soundings. Geophysics 70(4):H11–H19

Loke MH (2012) Tutorial: 2-D and 3-D electrical imaging surveys, 22 April 2012, Penang, Malaysia. http://www.geoelectrical.com/coursenotes.zip

Loke MH, Barker RD (1996) Rapid least-squares inversion of apparent resistivity pseudosections by a quasi-Newton method. Geophys Prospect 44:131–152

Loke MH, Dahlin T (2002) A comparison of the Gauss-Newton and Quasi- Newton methods in resistivity imaging inversion. J Appl Geophys 49:149–162

Loke MH, Acworth I, Dahlin T (2003) A comparison of smooth and blocky inversion methods in 2D electrical imaging surveys. Explor Geophys 34:182–187

Maiti S, Erram VC, Gupta G, Tiwari RK (2012) ANN based inversion of DC resistivity data for groundwater exploration in hard rock terrain of western Maharashtra (India). J Hydrol 464–465:281–293. doi:10.1016/j.jhydrol.2012.07.020

Maiti S, Gupta G, Erram VC, Tiwari RK (2013a) Delineation of shallow resistivity structure around Malvan, Konkan region, Maharashtra by neural network inversion of vertical electrical sounding measurements. Environ Earth Sci 68:779–794. doi:10.1007/s12665-012-1779-8

Maiti S, Erram VC, Gupta G, Tiwari RK, Kulkarni UD, Sangpal RR (2013b) Assessment of groundwater quality: A fusion of geochemical and geophysical information via Bayesian Neural Networks. Environ Monit Assess 185:3445–3465. doi:10.1007/s10661-012-2802-y

Mondal NC, Singh VP, Ahmed S (2013) Delineating shallow saline groundwater zones from Southern India using geophysical indicators. Environ Monit Assess 185:4869–4886

Mungale S (2001) Geology of the Chikotra basin with special reference to watershed development. Unpublished dissertation, Department of Geology, University of Poona 63

Park YH, Doh SJ, Yun ST (2007) Geoelectric resistivity sounding of Riverside alluvial aquifer in an agricultural area at Buyeo, Geum River watershed, Korea: an application to groundwater contamination study. Environ Geol 53:849–859

Pawar NJ, Pawar JB, Supekar A, Karmalkar NR, Kumar S, Erram VC (2009) Deccan dykes as discrete and prospective aquifers in parts of Narmada-Tapi Zone, Dhule district, Maharashtra. In: Srivastava RK, Sivaji Ch, Chalapathi Rao NV (eds) Indian Dykes: Geochemistry, Geophysics and Geochronology. Narosa Publishing House Pvt. Ltd., New Delhi, pp 189–198

Pazdirek O, Blaha V (1996) Examples of resistivity imaging using ME 100 resistivity field acquisition system. EAGE 58th Conference and Technical Exhibition Extended Abstracts Amsterdam

Rai SN, Thiagarajan S, Ratnakumari Y (2011) Exploration of groundwater in the basaltic Deccan traps terrain in Katol taluk, Nagpur district, India. Curr Sci 101(9):1198–1205

Rai SN, Thiagarajan S, Ratnakumari Y, Anand Rao V, Manglik A (2013) Delineation of aquifers in basaltic hard rock terrain using vertical electrical soundings data. J Earth Syst Sci 122(1):29–41

Ratnakumari Y, Rai SN, Thiagarajan S, Kumar D (2012) 2D Electrical resistivity imaging for delineation of deeper aquifers in a part of the Chandrabhaga River basin, Nagpur District, Maharashtra, India. Curr Sci 102(1):61–69

Ritz M, Parisot J-C, Diouf S, Beauvais A, Dione F, Niang M (1999) Electrical imaging of lateritic weathering mantles over granitic and metamorphic basement of eastern Senegal, West Africa. J. Appl Geophys 41:335–344

Singh KKK, Singh AKS, Singh KB, Sinha A (2006) 2D resistivity imaging survey for sitting water-supply tube well in metamorphic terrains: a case study of CMRI campus, Dhanbad, India. Lead Edge 25:1458–1460

Singhal BBS (1997) Hydrogeolo gical characteristics of Deccan trap formations of India. In: Hard rock hydrosystems. Proc. of Rabat symposium S2, vol 241, pp 75–80

Song SH, Lee JY, Park N (2007) Use of vertical electrical soundings to delineate seawater intrusion in a coastal area of Byunsan, Korea. Environ Geol 52:1207–1219

VanNorstrand R, Cook KL (1966) Interpretation of resistivity data. USCGS Professional Paper-499, US Govt. Printing Office, Washington

Zarroca M, Linares R, Bach J, Roqué C, Moreno V, Font L, Baixeras C (2012) Integrated geophysics and soil gas profiles as a tool to characterize active faults: the Amer fault example (Pyrenees, NE Spain). Environ Earth Sci 67:889–910

Zarroca M, Linares R, Roqué C, Rosell J, Gutiérrez F (2014) Integrated geophysical and morphostratigraphic approach to investigate a coseismic (?) translational slide responsible for the destruction of the Montclús village (Spanish Pyrenees). Landslides. doi:10.1007/s10346-013-0427-z

Zhu T, Feng R, Hao J, Zhou J, Wang H, Wang S (2009) The application of electrical resistivity tomography to detecting a buried fault: a case study. J Environ Eng Geophys 14(3):145–151